



UNIVERSITY OF LEEDS

This is a repository copy of *Robotic additive manufacturing system for dynamic build orientations*.

White Rose Research Online URL for this paper:
<https://eprints.whiterose.ac.uk/152759/>

Version: Accepted Version

Article:

Fry, NR orcid.org/0000-0001-8249-3993, Richardson, RC and Boyle, JH orcid.org/0000-0002-4219-9383 (2020) Robotic additive manufacturing system for dynamic build orientations. *Rapid Prototyping Journal*, 26 (4). pp. 659-667. ISSN 1355-2546

<https://doi.org/10.1108/RPJ-09-2019-0243>

Reuse

Items deposited in White Rose Research Online are protected by copyright, with all rights reserved unless indicated otherwise. They may be downloaded and/or printed for private study, or other acts as permitted by national copyright laws. The publisher or other rights holders may allow further reproduction and re-use of the full text version. This is indicated by the licence information on the White Rose Research Online record for the item.

Takedown

If you consider content in White Rose Research Online to be in breach of UK law, please notify us by emailing eprints@whiterose.ac.uk including the URL of the record and the reason for the withdrawal request.



eprints@whiterose.ac.uk
<https://eprints.whiterose.ac.uk/>

Robotic Additive Manufacturing System for Dynamic Build Orientations

N. R. Fry, R. C. Richardson, J. H. Boyle
School of Mechanical Engineering, University of Leeds

Abstract

Purpose – To present a multi-axis Additive Robot Manufacturing System (ARMS) and demonstrate its beneficial capabilities.

Design/methodology/approach – ARMS was constructed around two robot arms and a Fused Filament Fabrication (FFF) extruder. We conducted quantitative experiments to investigate: the effect of printing at different orientations with respect to gravity; the effect of dynamically changing build orientation with respect to the build tray when printing overhanging features; the effect of printing curved parts using curved, conformal layers. We combine these capabilities to print an integrated demonstrator showing potential practical benefits of the system.

Findings – Orientation with respect to gravity has no effect on print quality; Dynamically changing build orientation allows overhangs up to 90° to be cleanly printed without support structures; Printing an arch with conformal layers significantly increases its strength compared to conventional printing.

Research limitations/implications – We have not addressed the challenge of automatic slicing algorithms for multi-axis printing. We show that ARMS could eventually enable printing of fully-functional prototypes with embedded components.

Originality/value – This work is the first to prove that the surface roughness of an FFF part is independent of print orientation with respect to gravity. The use of two arms creates a novel system with more degrees of freedom than existing multi-axis printers, enabling studies on printing orientation relationships and printing around inserts. It also adds to the emerging body of multi-axis literature by verifying that curved layers improve the strength of an arch which is steeply curved and printed with the nozzle remaining normal to the curvature.

Keywords - Robotics, 3D Printing, Additive Manufacturing, Multi-axis.

Paper Type - Research Paper

I. INTRODUCTION

ADDITIVE Manufacturing (AM) processes create mechanical structures through sequential deposition of small amounts of material that is typically deposited in flat planes that are stacked vertically in layers. This process has proven very effective for complex shapes, especially when including a sacrificial ‘support material’. However, the use of support structures wastes material, slows the process, and for some shapes becomes encased within the object. Furthermore, the conventional layer printing approach can introduce weakness due to a tendency for layer de-lamination.

We present a 12-axis Additive Robot Manufacturing System (ARMS) built around industrial robot arms, which prints high quality parts comparable to those made by conventional systems. The additional kinematic freedom of this system allows us to demonstrate that conventional FFF printing can be done in any orientation relative to gravity without affecting print quality. We then show the advantages of dynamically changing the direction of layer deposition (relative to the build tray) when printing overhanging features without support material and demonstrate the advantages of printing curved parts using layers that conform to its shape. Finally, we combine these techniques to produce an integrated demonstrator (a model airplane) with an embedded electric motor, printed in a single process with no support material.

II. BACKGROUND

Additive Manufacturing has had a huge impact on prototyping and manufacturing due to its significant advantages: it is digitally driven and tooling free, which increases the speed and flexibility of production, while reducing costs for low volumes. It can also produce complex parts, including internal features, which could not be produced using any other manufacturing method. There are however four major limitations: the need for

support material; rough surface finish due to steps; anisotropic strength; difficulty embedding functional components.

Part orientation can be optimised for a range of factors, including support usage (Yicha and Alain, 2013; Afrose *et al.*, 2016). But because conventional AM systems can only deposit layers in one direction, complex geometries may have no ideal solution. Part orientation can also be limited by other factors such as adhesion to the print bed. By allowing build orientation to be varied during printing, this optimisation can be carried out for smaller sections reducing the compromises required (Ren *et al.*, 2010; Lee, Wei and Chung, 2014; Peng *et al.*, 2016; Zhao *et al.*, 2018).

Non-planar layers have previously been shown to improve surface finish and strength using conventional AM hardware. Singamneni and Huang (Huang and Singamneni, 2012; Singamneni *et al.*, 2012) were the first to do this, printing very shallow curved arches and comparing these with the same shape printed with horizontal planar layers. The curved layer arches were found to be up to 52% stronger. The effect of curved layers on surface roughness has not been quantitatively assessed, but a qualitative improvement in surface finish has been observed (Llewellyn-Jones, Allen and Trask, 2016). However, a conventional 3-axis system is fundamentally limited to shallow curves because the extruder orientation cannot be altered. An AM system with greater degrees of freedom is required to achieve greater surface angles, termed here as multi-axis additive manufacturing (MAAM). Previous MAAM systems have been based on three main types of mechanism, namely parallel robots (Song, Pan and Chen, 2015; Peng *et al.*, 2016; Yerazunis, Barnwell III and Nikovski, 2016), Cartesian stage systems (Lee, Wei and Chung, 2014; Tsao *et al.*, 2017) and serial robot arms (Brooks *et al.*, 2016; Tam and Mueller, 2017; Wu *et al.*, 2017; Kubalak, Wicks and Williams, 2019). The parallel and cartesian mechanisms are typically low cost systems, with limited motions, and none can control the pose of both the extruder and the build plate. Work using robotic arms has demonstrated that they are a promising platform for MAAM by showing larger scale prints and strength improvements (Tam and Mueller, 2017; Kubalak, Wicks and Williams, 2019), but the arms can suffer from low resolutions. In this work we have built a precise and flexible system that enables the study of mechanical characteristics of sample parts, which are of comparable quality to those from typical FFF printers, and the study of a greater range of printing orientations.

Embedding functional components within an additively manufactured robot, such that it works straight off the print bed, is seen as the next grand challenge in Additive Manufacturing (Gershenfeld, 2012; Lipson, 2015). This would be a significant advancement for AM as it extends the technology from purely mechanical structures to functional mechatronic devices, which could be readily customised and printed on demand. This could revolutionise manufacturing in areas where there are limited supply chains or where devices are required to adapt to changing needs, for example in search and rescue operations or remote medical centres. Embedding objects has been shown using Shape Deposition Modeling, a hybrid additive manufacturing method, but the inserts must be sealed to protect them from immersion in resin (Cutkosky and Kim, 2009). Others have used Shape Converters to allow inserts to be compatible with the limited motions of 3-axis printers (Kataria and Rosen, 2001). More recently research has been experimenting with printed electronic interconnects and constructing electro-mechanical components. One notable group at the University of Texas at El Paso have created a brushless motor by embedding components during the print cycle (Aguilera *et al.*, 2013). This work shows the promise of combining embedding, AM and electronics but the use of conventional flat layers limits the components shapes that can be embedded. In this work we show how additional assembly steps or reliance on simple component shapes could be eliminated when a dexterous extruder can print directly around complex objects.

III. ARMS SYSTEM ARCHITECTURE

There are 3 primary elements of ARMS: the robotic hardware enable motion; the printing mechanism to deposit material; and the software and control architecture to drive and synchronize the system.

Robot Hardware

ARMS uses two Denso VS-068 6-axis robot arms precisely located on a 1.5m x 1.5m steel anti-vibration base plate. The arms are relatively small but fast and precise (reach of 710mm; maximum payload of 7kg; maximum composite speed of 11m/s; position repeatability of ± 0.02 mm). The robots are designated as Extruder Robot (R_E) and Build Plate Robot (R_P) as shown in Figure 1a.

Printing Mechanism

ARMS deposits material via a Fused Filament Fabrication (FFF) process (using 1.75mm PLA filament and fan-assisted cooling). FFF was selected due to the potential impact MAAM could have on its major limitations, and the fact that it lends itself to printing directly onto existing structures.

Kinematics

The extruder and build plate robots are mathematically linked, along with the current G-code coordinate, into one 18 degree of freedom (DOF) kinematic chain as shown in Figure 1a and b. This allows the nozzle to be positioned relative to the build plate, irrespective of the build plate pose. R_E , R_P , and the printed object, O , are each described using Denavit-Hartenburg (D-H) notation, while the position and orientation of R_P 's base is described relative to R_E 's base.

R_E has the extruder assembly attached to its wrist such that the end of the tool frame corresponds with the tip of the nozzle. R_P holds the build plate and has a very similar kinematic chain to R_E . The printing instructions for a part are specified in modified G-code, which lists the coordinates (like standard G-code) and orientations (required for multi-axis printing) of the nozzle. These coordinates are relative to the build plate origin and are represented as a chain of links in D-H notation (see Fig. 1b). This set of links is added to R_P 's kinematic chain giving a mathematical representation of the G-code coordinate, in relation to the known physical location of the arm. To calculate the required joint angles for R_E , the known joint angles of R_P , desired positions from the G-code and relative positions of the robot's bases are combined to give one transformation matrix which relates P to the base of R_E (1).

$$T_{R_E} = T_B T_{R_P} T_O \quad (1)$$

Inverse Kinematics, K^{-1} , are used to calculate the joint angles, E , required for R_E to achieve this configuration (2). The tolerances for the solver were tuned until the worst-case position error fell below 0.05mm. These values, along with extruder commands, are sent to the hardware which prints a small section of the part. The process is then repeated for the next line of G-code.

$$E = K^{-1}(T_{R_E}) \quad (2)$$

Software and Control Architecture

The system architecture is composed of the subsystems shown in Figure 1c. The core control system is a bespoke LabVIEW program, which communicates with the other sub-systems and performs most of the computational work, including parsing the G-code and performing the kinematic calculations for the arms. Low-level control of the robot arms is accomplished by Denso RC8 computer controllers. A microcontroller drives the stepper motor on the extruder and runs a PID loop to control the nozzle temperature.

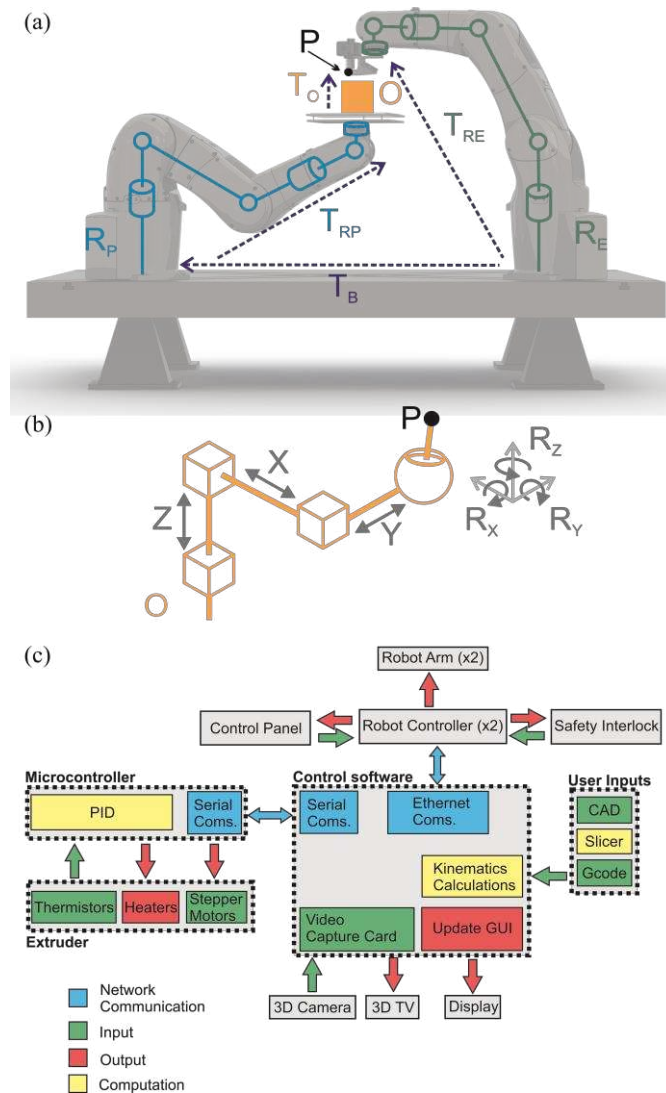


Fig. 1. (a) Side view of system showing the Build Plate (R_P), and Extruder (R_E) robots, the printed object (O) and the current G-code point (P). Links and rotary joints are overlaid onto each robot. The homogeneous transformations, created from the kinematic models, are shown as dashed arrows. (b) A close up of the kinematic links of the printed object (O) which are used to define the position and orientation of the current G-code point (P) in relation to the build plate. (c) A schematic of the ARMS system architecture showing the main hardware devices, software components, and the data flow as they communicate.

IV. ARMS FOR MULTI-AXIS PRINTING

ARMS offers the ability to research many new AM possibilities. We first investigate the impact on surface quality of printing in unconventional build directions, then assess the potential of two advantageous techniques. A technique termed '*Dynamic Build Orientation*' allows the planes in which material is deposited to be altered during the print process. Another, termed '*Conformal Layers*', makes it possible to print with curved layers.

V. FFF PRINTER ORIENTATION EFFECTS

Before addressing Dynamic Build Orientation, an experiment was first undertaken to establish whether the outcome of the FFF process is affected by having the extruder in an orientation other than vertical. Typically build orientation optimisation research is concerned with rotating the object to be printed within the build volume while the build plate remains horizontal and the extruder vertical.

In this experiment the whole process is rotated with the relative orientations of the part, bed and nozzle remaining the same (Fig. 2a). The build plate was repositioned by R_B so the part could be printed in five different orientations (0° , 45° , 90° , 135° , 180° from vertical, Fig 2b). In all cases the nozzle was normal to the print bed and the G-code was generated using typical slicing software (Slic3r) and settings (Table I). An overhanging curve comprised of five flat sided sections which are angled progressively further from vertical (up to 80°) was used for quantitative tests (Fig. 2a & d) and the surface quality was assessed by contact surface roughness measurement on the underside of each overhanging section. Four samples were printed at each orientation and surface roughness measured by three passes per section (Taylor-Hobson Form Talysurf 120L, $2\mu\text{m}$ conical stylus, 2.5mm cutoff, 100:1 bandwidth).

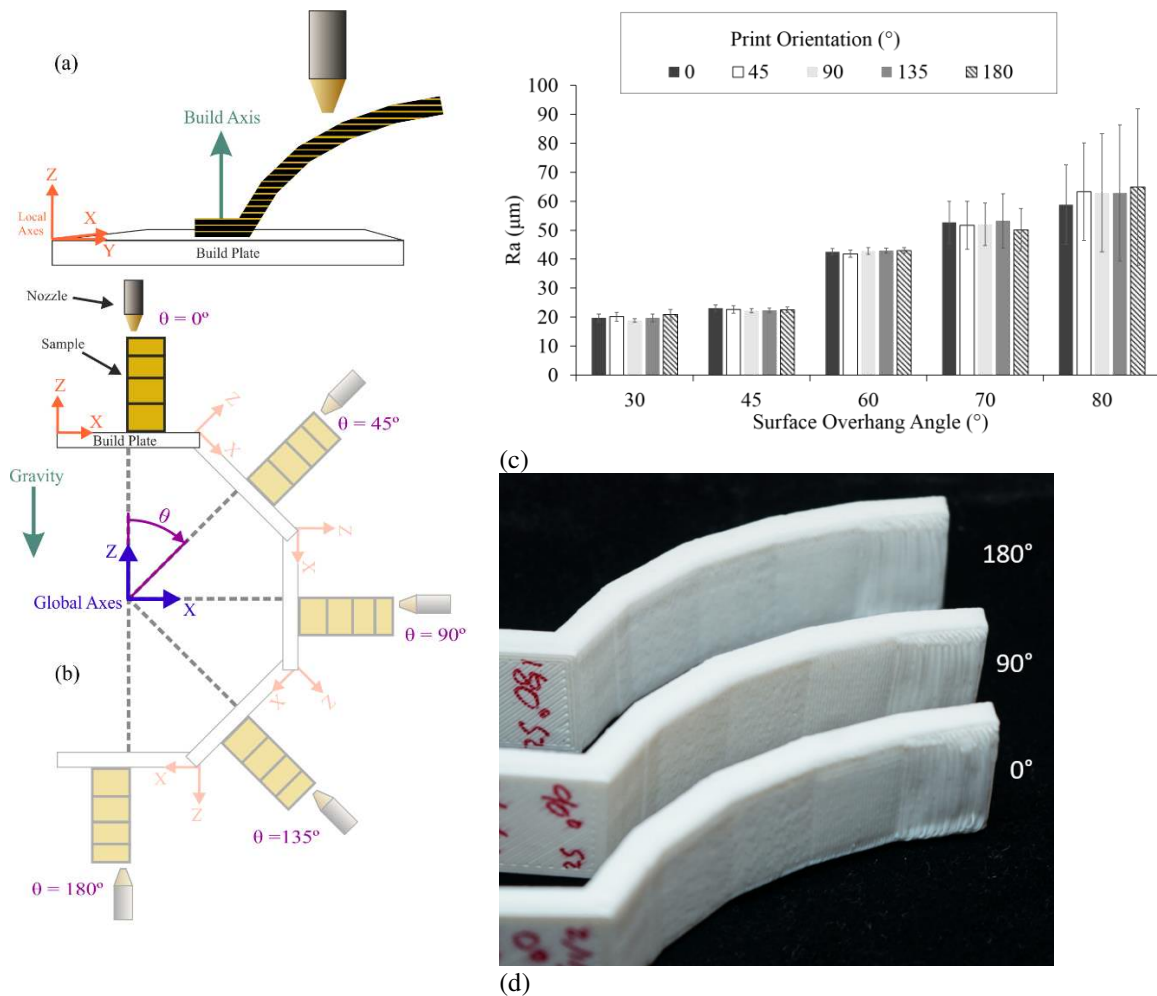


Fig 2. (a) Schematic showing the relative orientations of the build plate, nozzle and layers while the overhanging sample is printed. (b) The orientation of the print process is changed by rotating the bed θ around the global Y axis for each set of prints (c) Mean Ra values (n=12) for samples printed at each printer orientation. (d) Photograph showing the undersides of representative samples printed at $\theta=0^\circ$, 90° and 180° .

TABLE I
SLICER SETTINGS FOR PRINTER ORIENTATION EXPERIMENT

| Setting | Value |
|-----------------------|-----------------------|
| Layer Height | 0.2mm |
| Print Speed | 80mm/s |
| Temperature | 200°C |
| Material | Polymaker PolyMax PLA |
| Cooling | On |
| Infill Density | 20% |
| Infill Pattern | Honeycomb |
| Perimeters | 3 |
| Top and Bottom Layers | 6 |

Results

As shown in Fig. 2c, the Overhang Angle has a significant effect ($p < 0.05$) on surface roughness, as expected. The overall Printing Orientation, however, has no significant effect ($p = 1.00$) on roughness, with no statistically significant difference between any of the printing orientations tested ($p \geq 0.987$ in all cases). This is visually seen in Fig. 2d. There is also no significant interaction ($p = 0.99$) between the two main effects.

VI. DYNAMIC BUILD ORIENTATION

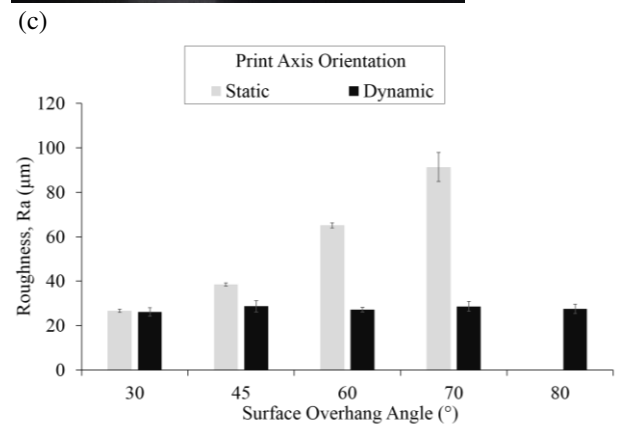
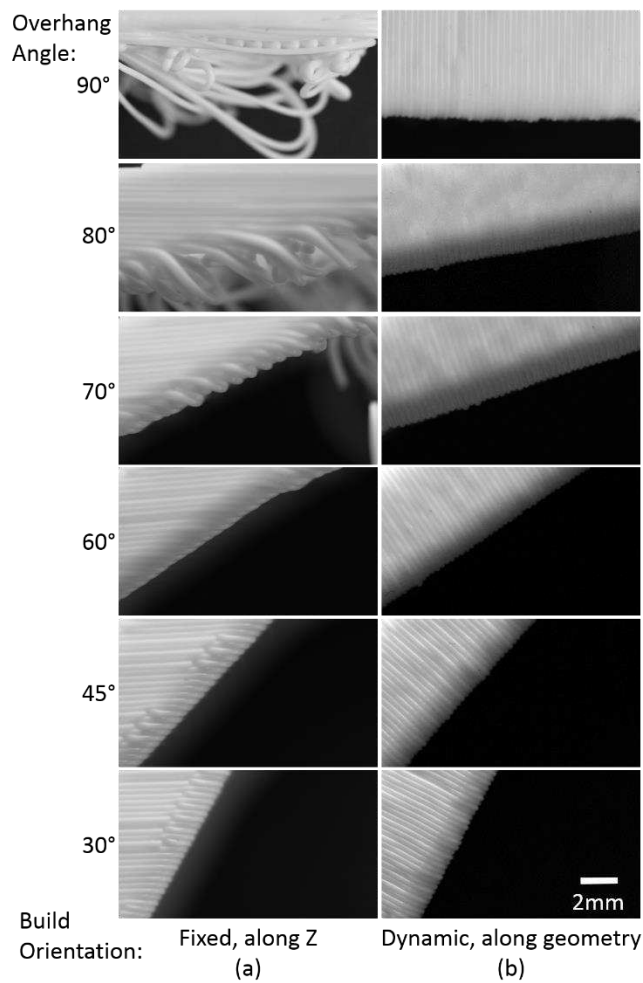
Dynamically altering the build orientation (the plane in which material is deposited) during a single print was investigated as it allows each section of a part to be printed in an orientation that optimizes print quality (quantified here with respect to surface roughness) and create features that would normally require the use of support material. The test piece with five increasing overhangs ($0^\circ - 80^\circ$) was again used to assess the impact upon surface roughness. Once the efficacy of the approach has been proven a single sample with a 90° section was produced to showcase this capability visually. The slicing angle was kept normal to the overhang angle for each section, theoretically keeping the roughness to a minimum throughout. The corresponding G-code was created by manually sectioning the design in CAD software (Solidworks), then slicing individual sections in the appropriate orientation (Simplify3D, settings in Table II) before rotating, translating and combining the codes using a LabVIEW program. This also added instructions (specific to ARMS) which set the orientation of the extruder nozzle to be perpendicular to the layers for the upcoming section. Samples for quantitative testing ($0^\circ - 80^\circ$) were printed three times each. For the control (conventional horizontal layers, Fig. 3a) standard slicing software (Simplify3D) was used. These control samples were printed on a conventional printer (Ultimaker 2+) to give a direct comparison with typical FFF results.

Results

The qualitative test confirmed that the dynamic orientation approach makes it possible to print even 90° overhangs cleanly, with no rough edges or drooping layers, without the need for support material (Fig. 3b). In the case of the 90° control sample (Fig. 3a), the plastic strands ultimately build up to the point that they can support further layers, but the underside is extremely poor quality with large drooping strands. If the 90° section were longer, it would ultimately fail completely. These qualitative observations are supported by the quantitative roughness results performed on the five-section samples ($0^\circ - 80^\circ$) and presented in Fig. 3d. Mean Ra depends heavily on overhang angle in the control prints, but remains constant when dynamically varying the build orientation. Note that the 80° section of the control samples were too rough to measure using the Talysurf's stylus.

TABLE II
SLICER SETTINGS FOR DYNAMIC BUILD ORIENTATION EXPERIMENT

| Setting | Value |
|-----------------------|-----------------------|
| Layer Height | 0.3mm |
| Print Speed | 30mm/s |
| Temperature | 200°C |
| Material | Polymaker PolyMax PLA |
| Cooling | On |
| Infill Density | 20% |
| Infill Pattern | Honeycomb |
| Perimeters | 2 |
| Top and Bottom Layers | 3 |



(d)

Fig. 3. Close-up images from the side of overhang arch samples showing (a) how the layers of the control sample remain horizontal and the edges droop increasingly as the overhang angle increases, due to reduced overlap with the previous layer. Conversely (b) shows the layers staying perpendicular to the overhang angle in the dynamic orientation sample, so all the edges are uniform. (c) A wider view of the control and dynamic build orientation 0° - 90° samples (d) Roughness measurements of the underside overhanging surface of 5 section (30-80°) samples printed with a static and dynamically varying orientations. Beyond 70° the static orientation samples were too rough to perform roughness measurements. Error bars show standard deviation, n = 9.

VII. CONFORMAL LAYERS

The multi-axis capabilities of ARMS make it possible to print with curved, non-planar layers. Here we investigate increasing the strength of a curved part by printing it with layers that conform to its shape.

Sample Preparation

A curved arch was chosen as the test sample for these experiments. Two sets of arches were printed, a control set (printed conventionally, Fig. 4a) and a conformal set (in which the shape of each layer matches the shape of the arch, Fig. 4b). The G-code for the control arches was created by slicing a 3D model in standard software (Simplify3D), including the necessary support structure. The conformal arch G-code was generated by a custom MATLAB script which used a mathematical description of the shape to generate the points for each layer, including the required nozzle orientation normal to the surface at each point. These points were offset vertically to create additional layers. G-code for the support structure was created conventionally (Simplify3D). This support was printed first, then covered with a thin layer of BuildTak (an adhesive-backed polymer sheet sold as a printing surface for FFF). This was done to avoid embossing the bottom surface with ridges due to stair-stepping of the support structure. Figure 4c shows a conformal arch being printed onto a build plate which is raised up from the wrist of the second robot (not shown) to give a greater range of collision-free poses. Five copies of each arch were printed.

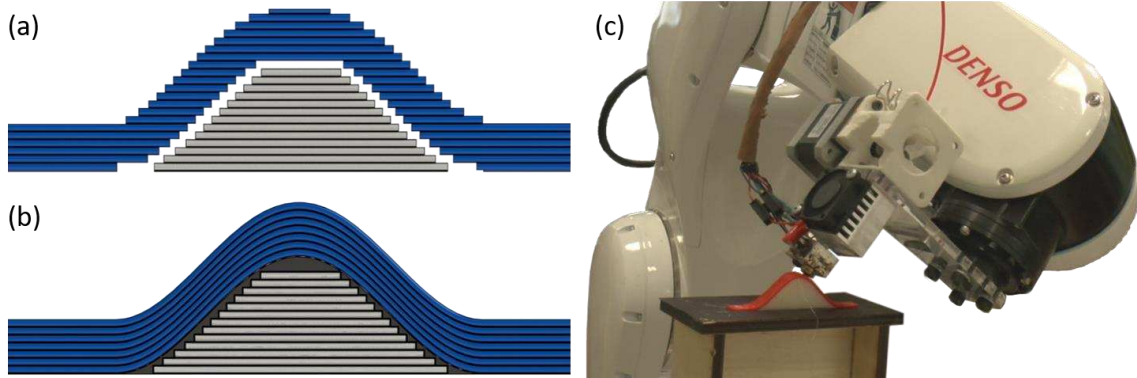


Fig. 4. Conformal layer experiments control samples (a) were printed using standard flat horizontal layers to approximate the curve, resulting in the characteristic stair step effect. The conformal samples (b) use layers which follow the shape of the arch. The black layer represents the smooth BuildTak which is used to cover the support structure prior to printing the arch itself. (c) A photograph taken during a conformal print illustrates how the multi-axis capabilities of ARMS make it possible for the nozzle to remain perpendicular to the surface being printed, even at steep angles.

Strength Tests

To determine the strength difference between the two construction techniques, tensile tests were performed. The arches were gripped by the flat ‘feet’ at each side and pulled at a constant speed of 5mm/min using an Instron 3369 tensile testing system. The tension vs. extension data was recorded, and the peak force before breakage was extracted.

Results

The conformal arches proved to be 57% stronger than the control arches, achieving an average maximum load of 184N versus 117N before breaking (Table III).

TABLE III
MAXIMUM TENSILE FORCE (N) FOR EACH ARCH SAMPLE

| Sample No. | Flat Layers | Curved Layers |
|--------------------|-------------|---------------|
| 1 | 121.36 | 161.45 |
| 2 | 124.57 | 207.65 |
| 3 | 91.37 | 170.62 |
| 4 | 116.38 | 198.82 |
| 5 | 131.41 | 180.32 |
| Mean | 117.02 | 183.77 |
| Standard Deviation | 15.34 | 19.23 |

VIII. INTEGRATED DEMONSTRATOR

An airplane body was printed around a motor to demonstrate the integration of the above techniques. *Conformal Layers* was applied to print around a cylindrical motor with attached propeller, while *Dynamic Build Orientation* made it possible to print the fuselage and wings without the use of supports.

Extruder modification

The previously used extruder (visible in Fig 4c) was too bulky, leading to collisions when attempting to print around the motor. A new, much slimmer extruder (visible in Fig. 5) from an inexpensive desktop 3D printer (CoLiDo D1315) was fitted and the motor was relocated to the second link of the robot, with the filament fed through a Bowden Tube.

Embedding the motor

The plane's propeller was fixed to a low-cost DC motor with a diameter of 24mm, which was clamped, nose-down, into a jig (visible in Fig. 5a). Printing directly onto the motor requires careful control of extruder orientation so that only the nozzle tip contacts the surface. In this case the extruder is kept at a 45° angle from vertical while also pointing towards the center of the cylinder (see Fig. 5a & b). As each circle of plastic is printed, the extruder orientation is constantly varied to maintain those criteria. A thin wall of material was printed around the motor along with additional features to secure it in place and mate with the front of the airplane fuselage. The G-code instructions specifying the nozzle positions and orientations required to embed the motor were created using a MATLAB script.

Printing Fuselage and Wings

The rest of the airplane is based on a CAD file for a model Spitfire (from (Mubin, 2017)) which we cut into three pieces (fuselage, left wing, right wing). The G-code for the fuselage was created using a standard slicer (Simplify3D) in "vase mode", giving a thin-walled hollow shell. The fuselage is printed directly onto the rim of the motor housing. The wings were individually sliced in the same way, before the resulting G-code was rotated and offset to the correct position and orientation using a custom LabVIEW program. The build axes for the wings are perpendicular to that for the fuselage, allowing them to be printed without support material. The orientation of the build plate is changed before printing each wing, in order to keep the print within the extruder robot's workspace. The key phases of this process can be seen in Figure 5 and Supplementary Movie S1.

Results

Using the techniques described, a model plane with an embedded DC motor was successfully manufactured in one continuous print. No pauses or interventions were required, and total print time was 3h 43m. The plastic was able to conform well to the motor, forming an integrated lip underneath and holding it firmly in place. The wings adhered well to the sides of the fuselage and the surface was smooth. Crucially, no support material or post processing was required. The plane was not designed to be functional, lacking a horizontal stabilizer and sufficient thrust to weight ratio, but the motor was able to spin the propeller when connected to a power source.

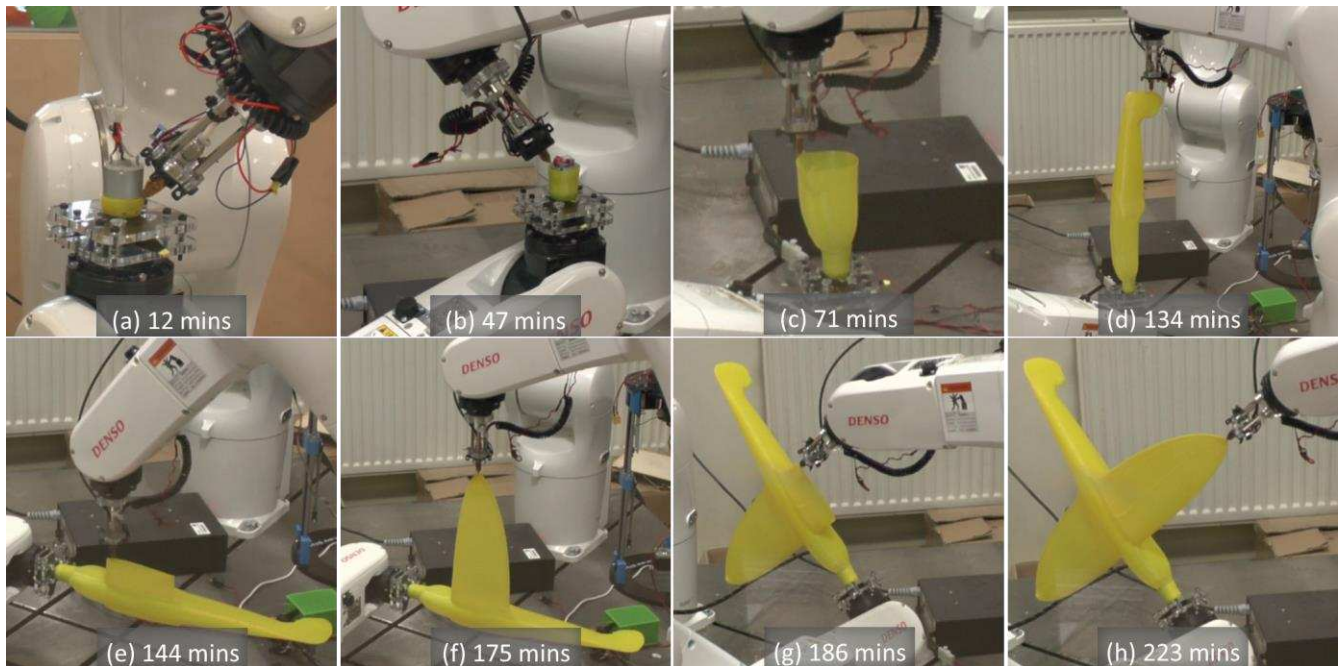


Fig. 5. Model aircraft fabricated with an embedded actuator and no support structures. (a) The propeller was attached to the motor beforehand and clamped in a jig. The nozzle is continuously angled at 45° away from the motor so that it can print against the motor's vertical side. (b) Motor is fully embedded. (c) Nozzle vertical and build plate lowered to increase the build volume. (d) Fuselage printed hollow as one continuous wall. (e) Fuselage is rotated so that the left wing can be built vertically removing any need for printing supports. (f) Nozzle kept vertical while printing the left wing. (g) Plane rotated backwards so that there is enough working room between the robots. The right wing cannot be printed vertically as the 1st wing would touch the base plate, therefore the nozzle is angled to be perpendicular to the fuselage, again removing the need for supports. (h) Plane completed in one continuous print process.

IX. DISCUSSION

One aim of creating this system was to enable the investigation of how multi-axis Additive Manufacturing affects the fundamentals of FFF. This is because previous work as shown the concept to be sound but has not tested underlying assumptions or demonstrated the theoretical benefits thoroughly with physical parts. The first result presented here shows that the surface roughness of an overhanging surface is not affected by its orientation with respect to gravity. This may be unexpected and demonstrates that the typical vertical orientation of the extruder in other systems is an unnecessary constraint. To understand why this is the case one must consider how a FFF extruder works. A spool of solid plastic filament is steadily pushed into a heated nozzle, where it melts and the molten plastic is deposited as a thin layer. Due to the force pushing the filament into the nozzle, the molten plastic is pressurised and will exit the nozzle, irrespective of the orientation it is in. When there is a surface one layer height away from the nozzle tip the plastic is forced onto this surface where it rapidly solidifies. As the overhang angle gets steeper there is less of an overlap between the edge of the previous layer and the new deposit, causing some of the plastic to be deposited in open air. This is why the roughness increases as the overhang increases. When the orientation is vertical, the assumption is made that gravity causes these unsupported edges to droop downwards, until you get to the extremes seen in Fig. 3a. Our results, however, indicate that the feed pressure of the plastic has a much greater influence than gravity as these 'drooping edges' are seen even when printing upside down. A hypothesis naturally follows that the part printed upside down may actually be smoother as gravity counteracts some of this force. The results do not support this conclusion however. This could be due to the active cooling fan which solidifies the plastic before it is able to flow far. It is also noted that this possible smoothing effect would only be apparent at large overhang angles where whole strands of plastic are unsupported, but these surfaces could not be measured with the contact methods employed here.

Secondly, the dynamic build orientation experiment took advantage of the fact the layers could be deposited at any angle. By changing the orientation of the extruder the layers could be orientated in such a way that there were no steps and unsupported edges between layers. This gives the lowest roughness value. In this case the manual sectioning of the part limited the number of distinct orientations, but with an automated slicing algorithm the orientation could be continuously varied to achieve the minimum roughness for each feature throughout a part.

Thirdly, conformal layers are shown to be stronger than the planar equivalents. This was expected due to previous work with a 3-axis printer (Huang and Singamneni, 2012; Singamneni *et al.*, 2012), but extends this work to show how more degrees of freedom enable steeper curvatures. FFF parts have anisotropic strength – the bonds between the layers are weaker than the layers themselves. The use of curved layers means that continuous tracks of plastic are printed along the axis which will be subjected to tension. Therefore, the strength improvement is due to the reduction of inter-layer bonds in the direction of the applied force.

Finally, the possibility of embedding components is demonstrated, and combined with the other multi-axis advantages. This is significant as embedding components, combined with pick and place capabilities and AM electronics methods paves the way for automated additive manufacturing of functional mechatronic and robotic devices. The utility of 12 DOF is also apparent from this demonstration as the plane is larger than the maximum work space between the two arms. This is achieved by moving the plane so that only the section currently being printed is within this space. This experiment would benefit from an automated planning algorithm that ensures the robot arms can reach all of the required positions to print a part. In this case all motions were simulated beforehand, and adjustments done manually before retesting. Work to address this aspect of MAAM is currently ongoing.

X. CONCLUSIONS

This paper has shown that ARMS is an effective and versatile multi-axis additive manufacturing system, which offers multiple advantages over conventional 3-axis FFF printers. In doing so we have shown that the precision of movement offered by commercially available industrial robot arms is more than sufficient to achieve high-quality 3D prints, making them an excellent foundation for future MAAM systems. Using the substantial kinematic freedom offered by the 12 DoF in ARMS, we conducted rigorous experiments that demonstrate fundamental capabilities and quantitatively evaluate the benefits they offer.

Our investigation of *FFF printer orientation effects* is, to the best of our knowledge, the first quantitative assessment of the effect of printing at different orientations relative to gravity. Somewhat counterintuitively, we find that gravitational orientation has no impact. This is an important finding in the context of MAAM because it means that both the extruder and build tray can be rotated as necessary to maximize workspace and optimize kinematics.

Our investigation of the *dynamic build orientation* capability shows that the angle of the layers, in relation to the feature being printed, has a significant effect on print quality. The roughness is at a minimum when the layers are perpendicular to the feature and increases, until the part becomes unprintable, when the angle of the layers tends towards the angle of the overhanging surface. ARMS's ability to dynamically vary the layer orientation as overhangs are printed overcomes this problem, allowing roughness to remain constant for any feature angle and eliminating the need for support material under overhangs.

It is well known that the bond between FFF layers is weaker than the material strength along layers, so layer orientation must be given special consideration when printing functional items where mechanical strength is important. It is sometimes possible to overcome this issue by changing the orientation of a part, but in general parts may include curved load bearing features for which no orientation of flat layers is optimal. Our investigation of the *conformal layers* capability demonstrated that ARMS is capable of printing steeply curved parts using conformal layers, and that doing so leads to significantly greater strength than conventional printing.

Finally, the production of our *integrated demonstrator* shows how the aforementioned capabilities could eventually be combined and applied to practical applications, such as printing a fully-functional robot prototype with embedded sensors, actuators and electronics.

XI. REFERENCES

- Afrose, M. F. *et al.* (2016) 'Effects of part build orientations on fatigue behaviour of FDM-processed PLA material', *Progress in Additive Manufacturing*, 1(1), pp. 21–28. doi: 10.1007/s40964-015-0002-3.
- Aguilera, E. *et al.* (2013) '3D printing of electro mechanical systems', in *Proceedings of the Solid*

Freeform Fabrication Symposium, pp. 950–961.

Brooks, B. J. *et al.* (2016) ‘Robot-assisted 3D printing of biopolymer thin shells’, *The International Journal of Advanced Manufacturing Technology*, pp. 1–12. doi: 10.1007/s00170-016-9134-y.

Cutkosky, M. R. and Kim, S. (2009) ‘Design and fabrication of multi-material structures for bioinspired robots’, *Philosophical Transactions of the Royal Society A: Mathematical, Physical and Engineering Sciences*, 367(1894), pp. 1799–1813. doi: 10.1098/rsta.2009.0013.

Gershenfeld, N. (2012) ‘How to make almost anything: The digital fabrication revolution’, *Foreign Aff.*, 91, p. 43.

Huang, B. and Singamneni, S. (2012) ‘Alternate slicing and deposition strategies for fused deposition modelling of light curved parts’, *J. of Achievem in mat and manuf*, 55(2), pp. 511–517.

Kataria, A. and Rosen, D. W. (2001) ‘Building around inserts: methods for fabricating complex devices in stereolithography’, *Rapid Prototyping Journal*, 7(5), pp. 253–262. doi: 10.1108/13552540110410459.

Kubalak, J. R., Wicks, A. L. and Williams, C. B. (2019) ‘Exploring multi-axis material extrusion additive manufacturing for improving mechanical properties of printed parts’, *Rapid Prototyping Journal*, 25(2), pp. 356–362. doi: 10.1108/RPJ-02-2018-0035.

Lee, W., Wei, C. and Chung, S.-C. (2014) ‘Development of a hybrid rapid prototyping system using low-cost fused deposition modeling and five-axis machining’, *Journal of Materials Processing Technology*, 214(11), pp. 2366–2374. doi: <http://dx.doi.org/10.1016/j.jmatprotec.2014.05.004>.

Lipson, H. (2015) ‘A Grand Challenge for Additive Manufacturing: Can We Print a Robot That Will Walk Out of the Printer?’, *3D Printing and Additive Manufacturing*, 2(2), p. 41.

Llewellyn-Jones, T., Allen, R. and Trask, R. (2016) ‘Curved Layer Fused Filament Fabrication Using Automated Toolpath Generation’, *3D Printing and Additive Manufacturing*, 3(4), pp. 236–243.

Mubin, N. (2017) *Supermarine Spitfire*. Available at: <https://grabcad.com/library/supermarine-spitfire-2> (Accessed: 15 August 2019).

Peng, H. *et al.* (2016) ‘On-The-Fly Print: Incremental Printing While Modelling’, in *Proceedings of the 2016 CHI Conference on Human Factors in Computing Systems*. ACM, pp. 887–896.

Ren, L. *et al.* (2010) ‘Integrated process planning for a multiaxis hybrid manufacturing system’, *Journal of manufacturing science and engineering*, 132(2), p. 21006.

Singamneni, S. *et al.* (2012) ‘Modeling and evaluation of curved layer fused deposition’, *Journal of Materials Processing Technology*, 212(1), pp. 27–35. doi: <http://dx.doi.org/10.1016/j.jmatprotec.2011.08.001>.

Song, X., Pan, Y. and Chen, Y. (2015) ‘Development of a Low-Cost Parallel Kinematic Machine for Multidirectional Additive Manufacturing’, *Journal of manufacturing science and engineering*, 137(2), p. 21005.

Tam, K.-M. M. and Mueller, C. T. (2017) ‘Additive Manufacturing Along Principal Stress Lines’, *3D Printing and Additive Manufacturing*. Mary Ann Liebert, Inc., publishers, 4(2), pp. 63–81. doi: 10.1089/3dp.2017.0001.

Tsao, C. *et al.* (2017) ‘Freeform Additive Manufacturing by vari-directional vari-dimensional material deposition’, *Rapid Prototyping Journal*.

Wu, C. *et al.* (2017) ‘RoboFDM: A robotic system for support-free fabrication using FDM’, in *2017 IEEE International Conference on Robotics and Automation (ICRA)*, pp. 1175–1180. doi: 10.1109/ICRA.2017.7989140.

Yerazunis, W. S., Barnwell III, J. C. and Nikovski, D. N. (2016) 'Strengthening ABS, Nylon, and Polyester 3D Printed Parts by Stress Tensor Aligned Deposition Paths and Five-Axis Printing', in *International Solid Freeform Fabrication Symposium*.

Yicha, Z. and Alain, B. (2013) 'Using AM feature and multi-attribute decision making to orientate part in Additive Manufacturing', in *High Value Manufacturing: Advanced Research in Virtual and Rapid Prototyping*. CRC Press, pp. 411–416. doi: doi:10.1201/b15961-7610.1201/b15961-76.

Zhao, G. *et al.* (2018) 'Nonplanar slicing and path generation methods for robotic additive manufacturing', *The International Journal of Advanced Manufacturing Technology*, 96, pp. 3149–3159. doi: 10.1007/s00170-018-1772-9.